UAB–LFAE 91–03
February 91

Precision Electroweak Results from ALEPH *

M. Martinez
CERN, CH-1211 Geneva, Switzerland
and
Laboratori de Física d'Altes Energies
Universitat Autònoma de Barcelona. E-08193 Bellaterra (Barcelona) Spain

Abstract

The analysis of the precision measurements of the Z^0 parameters obtained from the line-shapes and the asymmetries is presented. For that, data collected by the ALEPH detector in the runs in 1989-90 is used. The meaning of the measurements in terms of the Standard Model is discussed. Combining these measurements with the most relevant additional existing ones, information about the top mass is obtained.

1 Introduction

ALEPH has been designed as a general purpose detector for e^+e^- interactions and it is described in detail in reference [1]. In order to cope with this goal, ALEPH has been designed to have good track momentum resolution, fine calorimetric granularity, almost 4π angular coverage and hermeticity.

The ALEPH detector is shown in figure 1 and the characteristics of the relevant parts for the analysis presented in this report are described below. The detector has a $12 \times 12 \times 12$ m^3 cylindrical structure around the beam pipe with the interaction point in the center. It consists of two central tracking chambers: the *Inner Tracking Chamber* (ITC) mainly used for vertex determination and triggering, and the *Time Projection Chamber* (TPC) which is the main tracking detector and allows the determination of the momentum of charged particles with a resolution of $\Delta p/p \simeq 0.1\%$. Both are in a magnetic field of 1.5 T produced by a superconducting coil. Additionaly there are three calorimeters: the *Electromagnetic Calorimeter* (ECAL), which has a granularity of 1×1 degree and is used for detecting and measuring photons and electrons, the *Hadronic Calorimeter* (HCAL), for detecting hadrons and identifying muons (together with the *Muon Chambers*, which by the time being are not yet fully operational), and the *Luminosity Calorimeter* (LCAL), used to detect low angle Bhabha events in order to measure the integrated luminosity accumulated by the detector with a very small systematic error (less than 0.6%).

Other subdetectors which have not been used directly in this analysis but do play a very important role in the data acquisition are: The *Small Angle Tracking Device* (SATR), part of the luminosity monitor, used for verification of the LCAL alignment and as background monitor. The *Very Small Angle Luminosity Monitor* (BCAL), used to determine the instantaneous and

*Talk presented by M.Martinez at the XVIII International Meeting on Fundamental Physics and XXI G.I.F.T. International Seminar on Theoretical Physics on Precision Tests of the Standard Model at High Energy Colliders, Santander, 1990

specific luminosity and also as a background monitor. The *Vertex Detector*, not yet fully operational, but foreseen to provide a very accurate vertex tagging of tracks coming from the interaction point ($\sigma_{r\phi} = 13$ μm, $\sigma_z = 20$ μm).

A trigger system activates the readout of the detector for all observable Z decays. This trigger is based on three levels of decision which have to be passed in order to record the event. The rate of Z decays seen by ALEPH at a luminosity of 5×10^{30} cm^{-2}s^{-1} is about 0.18 Hz although the present trigger rate, including random triggers, is higher, of the order of 1 Hz.

A dedicated computer system, the *ALEPH Event Reconstruction Facility* (FALCON) provides a quasi-online event reconstruction of the data allowing a very fast availability of the data for analysis.

After a pilot run in August of 1989, LEP has delivered two running periods for physics data taking. The first took place between September and December of 1989, the second started in March 1990 and finished by Setember 1990.

In this report, both data samples recorded in 1989 and 1990 are included, corresponding to a total integrated luminosity of 7.7 pb^{-1}.

2 Selection of Z decay events

The basic feature of Z decay event selection is the extensive use of the TPC track multiplicity and momentum measurement. The good performance of our TPC together with the very low background rates allows a very simple and efficient event selection. The detailed description of the actual cuts used in each analysis can be found in reference [2].

2.1 Hadrons

The branching ratio of the Z into hadrons is of about 70% and therefore, hadron decay events dominate the information of the Z properties determination. Because of that, it is important to perform an analysis with very low systematic errors. Hadronic events from Z decays, are basically selected by requiring:

- high track multiplicity ($5 \leq N$) and
- minimum energy observed in the TPC of $\sum_i |p_i| \geq 0.1\sqrt{s}$ to reject two photon events

In the angular range $\cos\theta < 0.95$ the selection efficiency is $\epsilon = 0.975$. The results of this method are, in fact, combined with an alternative method using only calorimetry in such a way that the systematic error is reduced to $\Delta\epsilon = 0.002$ [2] being the background of less than 0.56%.

2.2 Leptons

The branching ratio of the Z into lepton pairs is only about 10%. Leptonic events, that is, e^+e^-, $\mu^+\mu^-$ or $\tau^+\tau^-$ pairs produced from an e^+e^- annihilation, have in contrast to hadrons, the following characteristic features:

- low track multiplicity ($2 \leq N \leq 10$) and
- very collinear and collimated back-to-back jet topology

Most electron and muon pairs appear as two track events, although in some cases more tracks are present due to photon conversions. Tau pairs are observed through the decay products of the tau particles. Most semileptonic tau decays, such as $\tau^- \to \nu_\tau \bar{\nu}_\mu \mu^-$, produce single tracks, but most hadronic tau decays, such as $\tau^+ \to \bar{\nu}_\tau \pi^+ \pi^+ \pi^- \pi^0$, produce multiple charged tracks.

The selection based upon the two aforementioned characteristics [2] has an efficiency of $\epsilon = 0.984 \pm 0.003$ inside the acceptance region and very small backgrounds coming from cosmic rays, two photon events and hadron decays amounting to less than 1.16% in total.

2.2.1 Lepton species tagging

Once the lepton pair events have been selected, the separation between the three possible species can be simply done by analyzing the charged momentum versus the total deposited calorimetric energy (see figures 2 for the Monte Carlo prediction and 3 for the data selected) and further improved by the detailed examination of each hemisfere to use the specific properties of each channel.

The electrons are characterized by high momentum together with high energy deposition in the calorimeters (most of it in the electromagnetic calorimeter except when the track penetrates through a crack, in which case the energy deposition is observed in the hadronic calorimeter).

The muons are also characterized by a high visible momentum but their signature in the calorimeters corresponds to that of a minimum ionizing particle. Also, they are clearly observed as outgoing tracks in the digital read-out of the HCAL and in the muon chambers.

Finally, the taus populate the medium and low range of visible energy and momentum, since a fraction of the tau energy is carried out by the emission of neutrinos and are well selected by studying the missing invariant mass.

2.2.2 Extracting Z decay information from $e^+e^- \to e^+e^-$

The final state in which an electron pair is observed does not give a direct information about the Z properties since the t-channel Bhabha scattering amplitude and its interference with the Z production amplitude plays an important role, which is specially enhanced:

- at low scattering angles and
- out of the peak.

Unlike for the s-channel driven processes (the rest of leptons and the hadrons), for $e^+e^- \to e^+e^-$ there is no available precise formulae [1] to extract Z decay information and therefore the following strategy has been followed:

- 1.- Use events in the range $-0.9 < \cos\theta < 0.7$ and only near the peak: $\sqrt{s} = M_Z \pm 1$ GeV to be sure that the t-channel effects are reasonably small.
- 2.- Use the most accurate available Bhabha calculations [4] to evaluate the "equivalent number of events" due to the additional t-channel contribution for each $\cos\theta$ and $\sqrt{s}$ in order to subtract them from the observed events. In the above ranges this corresponds to a total correction of $\sim 10\%$ for $e^+e^- \to e^+e^-$.

[1] A new fitting formula [3] has been recently developped to describe the process $e^+e^- \to e^+e^-$ with a precision comparable to the one used for the study of the s-channel processes. This formula has been recently applied to the ALEPH data showing a perfect agreement with the method described here within the quoted errors. It is plained the use of this new formula in the future analysis.

- 3.- To evaluate the systematic uncertainty introduced by this t-channel subtraction, extensive cross-checks of the different available calculation and of the effect of changing the electroweak parameters in the subtracted cross section are performed. At the time being, the largest differences observed amongst the different calculation suggest a safe estimate of an error $\sim 0.5\%$ of the correction applied.

Table 1 summarizes the basic trends of the event selection.

	$\cos\theta$	$\sqrt{s}$	Events	Eff.(in acc.)	BKGD	Sys.error
Luminosity		All points	~200 K			0.8%
Hadrons	-0.95/0.95	All points	~180 K	97.5%	0.56%	0.2%
e^+e^-	-0.9/0.7	$M_Z \pm 1$ GeV	~9 K	99.4%	1.18%	0.4%
$\mu^+\mu^-$	-0.9/0.9	$M_Z \pm 3$ GeV	~6 K	99.8%	0.47%	0.6%
$\tau^+\tau^-$	-0.9/0.9	$M_Z \pm 3$ GeV	~6 K	85.5%	1.45%	0.8%
Common leptons	-0.9/0.9	$M_Z \pm 1$ GeV	~25 K	98.4%	1.16%	0.3%

Table 1: Summary of the basic trends of the event selection.

3 Analysis of Z event properties

From the Z decay events we will concentrate our attention in two basic properties: for each center of mass energy we are interested in

- counting the number of events in order to extract the *cross section* and,
- for the leptonic decays also studying the angular distribution in order to fit the $\cos\theta$ dependence to compute the *charge forward-backward asymmetry.*

3.1 Cross sections

We will describe now how the cross section is obtained from the data and how its energy dependence is fitted to extract the relevant physical information.

3.1.1 Experimental Calculation

The calculation of the cross section for each decay type is performed by using the fact that at very low angles, the Bhabha cross section is essentially dominated by the t-channel photon exchange and therefore it is large and can be well described by QED being the dependence on the Z parameters very small. An specific subdetector is in charge of counting the low angle Bhabha rate (the *LCAL*) and the expected cross section has been carefully studied (see table 2) being known at present with an error of 0.8%.

The cross section for each decay type is then obtained by applying the simple formula

$$\sigma(s) = N_{corrected}(s)\,\frac{\sigma_{Bhabha}(s)}{N_{Bhabha}(s)} \qquad (1)$$

where $N_{corrected}$ is the number of events observed, corrected by efficiencies and acceptances and therefore corresponding to a perfect detector with 4π acceptance, N_{Bhabha} is the observed

Beam parameters and survey	0.0005
Apparatus uncertainties	0.0045
Monte Carlo statistics	0.0040
Total exp. error	0.006
Theoretical uncertainty	0.005
TOTAL	0.008

Table 2: Sources of systematic errors in the determination of the Bhabha cross section seen by the LCAL detector. This error propagates directly to the evaluation of the integrated Luminosity.

number of Bhabha events in the $LCAL$ and σ_{Bhabha} is the Bhabha cross section covered by the $LCAL$. The ratio $\frac{N_{Bhabha}}{\sigma_{Bhabha}}$ is in fact the integrated luminosity provided by LEP. The small dependence of σ_{Bhabha} on the Z properties is accounted for by using an iterative procedure: it is computed by using the fitted values of the Z parameters until the values converge (usually at the first iteration).

Figures 4 and 5 show the measured cross section as a function of the center of mass energy (lineshape) for hadrons and leptons respectively.

3.1.2 Theoretical description

The Z lineshape can be basically described by a radiatively distorted Breit-Wigner resonance. The initial state radiation has a very important effect in the lineshape (it reduces the peak cross section by about 30% and shifts the peak position by some 110 MeV) but is known at the level of few per mil precision and can be accounted for, by convoluting the non-radiative cross section with a suitable radiator function:

$$\sigma(s) = \int_0^{x_{max}} dx H(x,s) \sigma_{NR}(s(1-x)) \tag{2}$$

where $H(x,s)$ gives the probability of having a fractional energy lost due to initial state radiation of x and $\sigma_{NR}(s(1-x))$ is the non-radiative cross section computed at the reduced center of mass energy.

The radiator $H(x,s)$ is just a function of the electron mass m_e, the electromagnetic constant at the Thompson limit α_0, s and x so that it comes from a pure QED calculation which has been computed up to complete $O(\alpha^2)$ plus exponentiation of the leading infrared and virtual corrections [5].

Concerning the non-radiative cross section, since precision measurements have to be performed, it is important to use the most accurate description preserving its model independence. Assuming that the observed resonance is due to the amplitudes of the exchange in the s-channel of either an unique massive vector boson or a photon, and using just Quantum Field Theory principles and the well established QED theory, we can write [6]

$$\begin{aligned}\sigma_{NR}^f &= \frac{s\Gamma_Z^2}{(s-M_Z^2)^2 + \left(s\frac{\Gamma_Z}{M_Z}\right)^2}\left[\sigma_0^f \frac{1}{1+\delta_{QED}} + \frac{\bar{I}_f(s-M_Z^2)}{s}(1+Q_f^2\delta_{QED})(1+\delta_{QCD})\right] \\ &+ N_c^f \frac{4\pi\alpha^2(s)}{3s} Q_f^2 (1+Q_f^2\delta_{QED})(1+\delta_{QCD})\end{aligned} \tag{3}$$

being M_Z and Γ_Z the physical mass and width of the Z boson and σ_0^f the peak cross section for the production of fermion f which can be expressed in terms of the partial widths as

$$\sigma_0^f = \frac{12\pi}{M_Z^2}\frac{\Gamma_e\Gamma_f}{\Gamma_Z^2} \tag{4}$$

and being

$$\begin{aligned} \delta_{QED} &= \frac{3\alpha}{4\pi} \\ \delta_{QCD} &= \frac{\alpha_s(M_Z^2)}{\pi} + 1.405\left(\alpha_s(M_Z^2)\right)^2 \end{aligned} \tag{5}$$

the final state photon and gluon (only for $f = u, d, s, c, b$) radiation corrections respectively.

The factor $\bar{I}_f$ of the interference term can be treated in two different ways: it can be considered an additional physical parameter containing information independent from the parameters mentioned above, in which case it should be fit from the data; or one can try to obtain $\bar{I}_f$ from a deeper insight into the theory.

In the second approach, there is no way of writing $\bar{I}$ in terms of the physical parameters. Therefore one must actually break the model independence of the whole formula and specify a model for writing it. Within the Standard Model, the expression for $\bar{I}_f$ is, in leading terms,

$$\bar{I}_f = -\frac{4N_c^f\pi\alpha(s)\alpha(M_Z^2)Q_f}{3}\left(v_e(M_Z^2)\cdot v_f(M_Z^2)\right) \tag{6}$$

where the coupling v_f is

$$v_f(M_Z^2) = \frac{I_3^f - 2Q_f\sin^2\theta_W(M_Z^2)}{2\sin\theta_W(M_Z^2)\cos\theta_W(M_Z^2)} \tag{7}$$

$\sin^2\theta_W(M_Z^2)$ [2] being the universal effective weak mixing angle.

For realistic $\sin^2\theta_W(M_Z^2)$, the interference I is positive; and near the peak the whole term amounts to a very small fraction of the total cross section [6]. Therefore, one way to treat the term is to compute $\bar{I}_f$ for any reasonable value of $\sin^2\theta_W(M_Z^2)$ and consider the variation in the total cross section due to the difference with the actual value of $\sin^2\theta_W(M_Z^2)$ as just an uncertainty of the formula. Since this variation is small, we can say that the model independence is only very softly broken.

This formula gives a model-independent, very precise ($\simeq 0.1\%$ for hadrons and $\simeq 0.2\%$ for lepton [6]) description of the Z lineshape in terms of M_Z, Γ_Z and σ_0 or equivalently M_Z, Γ_Z, Γ_e and Γ_f.

3.1.3 Fitting procedure

To extract the lineshape information, assuming that all the decays are from the same Z resonance, the lineshapes are fitted together. In practice two kinds of fits are performed:

[2] The universal effective mixing angle has been defined by many authors [7] and called in different ways ($\sin^2\theta_W^*$,$\overline{\sin^2\theta_W}$, $\sin^2\widehat{\theta_W}(M_Z^2)_{\overline{MS}}$,...) being, in fact, all the definitions equivalent to a very good degree of accuracy, by far much larger than the one discussed here

- Hadrons + Taus + Muons + Electrons $\rightarrow$ 4 lineshapes $\rightarrow$ 6 parameters
- Hadrons + Leptons (universality assumed) $\rightarrow$ 2 (common leptons) or 4 (individual leptons) lineshapes $\rightarrow$ 4 parameters

In order to account for the correlations amongst the different lineshape data and amongst their errors, it is important to perform the fit minimizing the χ^2 difference between the measured values and their expectations defined in the most general way, namely:

$$\chi^2 = \sum_{i,j}^{total\ points} (\sigma_i - \sigma(s_i)) \cdot V_{ij}^{-1} \cdot (\sigma_i - \sigma(s_i)) \tag{8}$$

being σ the measured values,$\sigma(s)$ the theoretical expectations and V_{ij} is the expected full covariance matrix of the data, which can be easily computed to be

$$V_{ij} = \sigma(s_i) \cdot \sigma(s_j) \cdot \sum_k \left(\frac{\Delta c_k}{c_k}\right)^2 \tag{9}$$

where $i, j = 1, total\ points$ and c_k stands for all the common sources of error for σ_i and σ_j:

For the diagonal terms, $i = j$ then simply $\Delta c = \Delta\sigma_i$, the expected error. For the off-diagonal terms, $i \neq j$ then there are clearly three sources of common errors:

- *The Luminosity Systematic*, due to the error in the Bhabha cross section used for normalization and common to all points: $\left(\frac{\Delta c}{c}\right)_{LUMI} = 0.8\%$
- *The Specific Systematic* for the selection of each decay type (see table 1) which is common to all the points in each lineshape: $\left(\frac{\Delta c}{c}\right)_{SPECIFIC} = (0.2_{had.} \rightarrow 0.8_{tau})\%$
- *The Bhabha Normalization* at each energy, due to the fact that at each energy point, the same number of Bhabha events is used in all the lineshapes to normalize the cross section. Therefore it is common to all the points at the same center of mass energy. It can be easily proven that if for lineshape 1 at a given center of mass energy, the number of Bhabha events used for normalization is N_1 and for lineshape 2 is $N_2 \subset N_1$ then: $\left(\frac{\Delta c}{c}\right)_{BHABHA} = \frac{1}{\sqrt{N_1}}$

3.1.4 Results

There is a big freedom in choosing the parameters to express the results of the fits, but it is worth trying to use a set in which there is minimal correlation amongst them. This can be found after analyzing the actual independent physical information contained in the lineshapes. Our choice is the following:

- M_Z which gives us the peak position of the lineshapes
- Γ_Z which gives us the widths of the lineshapes
- σ_0^h which gives us the peak height of the hadronic lineshape (by far the best determined because of its larger statistic)
- $R = \frac{\sigma_0^h}{\sigma_0^l} = \frac{\Gamma_h}{\Gamma_l}$ which gives us the peak height ratio

All these parameters are essentially uncorrelated, with the exception of Γ_Z and σ_0^h which have a small correlation. From these parameters, any other can be easily computed propagating properly the errors.

The results of the 4 parameter fit are the following:

$$\begin{aligned} M_Z &= (91.182 \pm 0.009_{exp} \pm 0.02_{LEP})\ \text{GeV} \\ \Gamma_Z &= (2.488 \pm 0.017)\ \text{GeV} \\ \sigma_0^h &= (41.76 \pm 0.39) nb \\ \frac{\Gamma_h}{\Gamma_l} &= 21.07 \pm 0.19 \end{aligned}$$

being $\chi^2/NDF = 51/53$ and the only relevant correlation is $\rho_{(\Gamma_Z,\sigma_0^h)} = -0.29$. Equivalently we can write

$$\begin{aligned} \Gamma_l &= (83.3 \pm 0.7)\ \text{MeV} \\ \frac{\Gamma_{inv}}{\Gamma_l} &= 5.78 \pm 0.16 \end{aligned}$$

In the 6 parameter fit we obtain:

$$\begin{aligned} \frac{\Gamma_h}{\Gamma_e} &= 20.65 \pm 0.32 \\ \frac{\Gamma_h}{\Gamma_\mu} &= 21.50 \pm 0.31 \\ \frac{\Gamma_h}{\Gamma_\tau} &= 20.97 \pm 0.34 \end{aligned}$$

being $\chi^2/NDF = 47/51$. Table 3 shows the results in terms of different parameter set.

Final State	Partial Width (MeV)	Branching Ratio (%)	Peak cross section (nb)
hadrons	1756 ± 15	70.6 ± 0.5	41.76 ± 0.39
e^+e^-	84.2 ± 0.9	3.38 ± 0.03	2.022 ± 0.036
$\mu^+\mu^-$	80.9 ± 1.4	3.25 ± 0.05	1.942 ± 0.032
$\tau^+\tau^-$	82.9 ± 1.6	3.33 ± 0.06	1.991 ± 0.036
lepton	83.3 ± 0.7	3.35 ± 0.02	1.982 ± 0.025
invisible	481 ± 14		

Table 3: Results of the 4 and 6 parameter fits to the hadron and different lepton lineshapes in terms of different variables.

3.2 Forward-Backward asymmetry

Leptonic decays, given the fact that are detected as collimated back-to-back low multiplicity events, allow a clean charge identification and direction measurement of the fermions produced in the final state (in opposition with hadronic events where the determination of both variables is very difficult). We will describe now how the forward-backward charge asymmetry is obtained from the angular distribution of the leptonic data and how its energy dependence is fitted to extract the relevant physical information.

3.2.1 Experimental Calculation

It is clear that since initial state radiation tends to escape along the beam direction, it is worth studying the angular distribution of the outgoing particles in their center of mass frame. There, the distribution in terms of the center of mass polar angle can be written with very good approximation [8] in the following way:

$$\frac{d\sigma(s)}{d\cos\theta^*} = C \cdot \left((1+\cos^2\theta^*) + \frac{8}{3} A_{FB}(s)\cos\theta^*\right) \tag{10}$$

where C is an irrelevant normalization constant and A_{FB} is the forward-backward asymmetry, defined as

$$A_{FB} = \frac{\sigma_F - \sigma_B}{\sigma_F + \sigma_B} \tag{11}$$

with

$$\begin{aligned} \sigma_F &= 2\pi \int_0^1 d(\cos\theta)\, \frac{d\sigma}{d\Omega} \\ \sigma_B &= 2\pi \int_{-1}^0 d(\cos\theta)\, \frac{d\sigma}{d\Omega} \end{aligned} \tag{12}$$

For taus and muons A_{FB} is obtained directly from the data by using the measured polar angle $\cos\theta^*$ event by event to build the negative log-likelihood function

$$L(A_{FB}(s_i)) = -\sum_{k=1}^{N_i} \ln\left((1+\cos^2\theta_k^*) + \frac{8}{3} A_{FB}(s_i)\cos\theta_k^*\right) \tag{13}$$

where N_i is the total number of events at the energy s_i. The minimization of this function in terms of $A_{FB}(s_i)$ provides the actual asymmetry measured for this energy. It can be easily proven that in this procedure, the actual angular acceptance of the detector does not play any role.

For electrons, since the t-channel subtraction has to be done before trying to extract the genuine A_{FB} from the angular distribution, the data is already binned in $\cos\theta^*$ and therefore a minimization of the χ^2 is performed. Figure 6 shows the energy dependence of the measured asymmetries for each lepton species and for the common lepton selection.

3.2.2 Theoretical description

The existence of forward-backward charge asymmetry comes from the structure of the couplings, and therefore allows us to measure the size of the vector and axial vector couplings of the Z. Writing at the tree level the photon coupling to charged leptons as

$$-i\,e\,\gamma^{\mu} \tag{14}$$

and the Z coupling as

$$-i\,\frac{e}{2\sin\theta_W\cos\theta_W}\,\gamma^{\mu}(g_v^l+g_a^l\gamma^5) \tag{15}$$

then the radiatively corrected forward-backward asymmetry can be written in very good approximation [9] as

$$A_{FB}(s)=\frac{\int_1^{x_{max}}\frac{4(1-x)}{(2-x)^2}H(s,x)\sigma_{NR}^{FB}(s(1-x))}{\int_1^{x_{max}}H(s,x)\sigma_{NR}(s(1-x))} \tag{16}$$

being $H(x,s)$ the radiator function, like in the case of the total cross section. In the numerator, $\sigma_{NR}^{FB}=\sigma_{NR}^{F}-\sigma_{NR}^{B}$ is the integrated forward minus backward cross section, which in terms of effective couplings is

$$\sigma_{NR}^{FB}(s)=\frac{\pi\alpha^2(s)}{s}\;\Big(\quad 2\;\; g_a^e g_a^f F_G\frac{s(s-M_Z^2)+s\frac{\Gamma_Z}{M_Z}\Im(\Delta\alpha)}{(s-M_Z^2)^2+s^2\frac{\Gamma_Z^2}{M_Z^2}} \\ 4\;\; g_v^e g_a^e g_v^f g_a^f F_G^2\frac{s^2}{(s-M_Z^2)^2+s^2\frac{\Gamma_Z^2}{M_Z^2}}\;\Big) \tag{17}$$

whereas the denominator is the total cross section, which can be expressed as

$$\sigma_{NR}(s)=\frac{4}{3}\,\frac{\pi\alpha^2(s)}{s}\;\Big(\;1\;+\;2\,g_v^e g_v^f F_G\frac{s(s-M_Z^2)}{(s-M_Z^2)^2+s^2\frac{\Gamma_Z^2}{M_Z^2}}+ \\ ((g_v^e)^2+(g_a^e)^2)\;\cdot\;((g_v^f)^2+(g_a^f)^2)\;F_G^2\frac{s^2}{(s-M_Z^2)^2+s^2\frac{\Gamma_Z^2}{M_Z^2}}\;\Big) \tag{18}$$

being

$$F_G=\frac{\sqrt{2}G_F M_Z^2}{4\pi\alpha(s)} \tag{19}$$

Assuming the Standard Model, the couplings g_v^f and g_a^f can be expressed to a good accuracy as

$$\begin{aligned} g_v^f &= \rho_f^{\frac{1}{2}}\,(I_3^f-2Q_f(\sin^2\theta_W)_f) \\ g_a^f &= \rho_f^{\frac{1}{2}}\,I_3^f \end{aligned} \tag{20}$$

ρ_f and $(\sin^2\theta_W)_f$ being the flavour-dependent effective rho parameter and weak mixing angle at M_Z^2 respectively.

At the peak, where most of the statistics is accumulated, the previous expression simplifies for leptons to

$$A_{FB} \simeq \frac{3}{4} \cdot \frac{2g_v^e g_a^e}{(g_v^e)^2 + (g_a^e)^2} \cdot \frac{2g_v^f g_a^f}{(g_v^f)^2 + (g_a^f)^2} \sim 3\frac{(g_v^l)^2}{(g_a^l)^2} \tag{21}$$

so that the basic information that comes out of the asymmetry measurement is the squared of the ratio of the vector over the axial Z couplings.

3.2.3 Fitting procedure

Since the errors on the asymmetries fitted are still large, we assume universality and fit simultaneously the s dependence of the asymmetries of each lepton final state in terms of just four parameters: M_Z, Γ_Z, $(g_v^l)^2$ and $(g_a^l)^2$. Additionaly we use as constrains the, by far, more precise lineshape measurements:

- $M_Z \pm \Delta M_Z$ which effectively fixes M_Z
- $\Gamma_Z \pm \Delta\Gamma_Z$ which effectively fixes Γ_Z
- $\Gamma_l \pm \Delta\Gamma_l$. Since we can express $\Gamma_l = \frac{G_F M_Z^3}{6\pi\sqrt{2}}((g_v^l)^2 + (g_a^l)^2)(1 + \delta_{QED})$ but $(g_v^l)^2 \ll (g_a^l)^2$ this means that we are effectively fixing $(g_a^l)^2$, which is directly related to the slope of the energy dependence of the asymmetry

3.2.4 Results

The results of the fits are the following:

$$\begin{aligned} \left(\frac{g_v^l}{g_a^l}\right)^2 &= (0.82 \pm 0.26) \times 10^{-2} \\ (g_a^l)^2 &= 0.2484 \pm 0.0022 \end{aligned}$$

being $\chi^2/NDF = 32/32$. Equivalently we can express

$$\begin{aligned} (g_v^l)^2 &= (0.203 \pm 0.065) \times 10^{-2} \\ (g_a^l)^2 &= 0.2484 \pm 0.0022 \end{aligned}$$

or

$$\begin{aligned} g_v^l &= -0.0451 + 0.0079 - 0.0070 \\ g_a^l &= -0.4984 \pm 0.0022 \end{aligned}$$

Another interesting way of expressing the results is by quoting the fitted value of the peak asymmetry and the lepton partial width:

$$\begin{aligned}(A_{FB}^l)_{peak} &\equiv \frac{3}{4}\cdot\left(\frac{2g_v^l g_a^l}{(g_v^l)^2+(g_a^l)^2}\right)^2 = 0.024 \pm 0.008\\ \Gamma_l &= (83.2 \pm 0.7)\ \text{MeV}\end{aligned}$$

Assuming the Standard Model structure of the couplings, the results can be also expressed in terms of ρ_l and $(\sin^2\theta_W)_l$:

$$\begin{aligned}\rho_l &= 0.9935 \pm 0.0087\\ (\sin^2\theta_W)_l &= 0.2274 + 0.0040 - 0.0036\end{aligned}$$

Figure 7 shows the 1 σ and 2 σ confidence level contours in the plane g_v^l versus g_a^l. The fact that we only measure $(g_v^l)^2$ is the reason for having symmetric regions in g_v^l.

4 Comparison with the Standard Model predictions

We can use our most precise measurement, M_Z, which has an error of only $\Delta M_Z/M_Z < 0.025\%$ together with the already existing ones

$$\alpha_0 \qquad G_F \qquad m_{f\neq t}$$

to compare the rest of our measurements with any theoretical model. Given these inputs, any observable in the minimal Standard Model is just a function

$$f = f(\alpha_s, m_t, m_H; N_\nu)$$

so that it depends on a badly known quantity, α_s, two unknown ones, m_t and m_H and the value of the number of neutrino species N_ν.

- α_s affects mainly only hadronic observables. The value that we use is the one obtained from the extrapolation of the QCD correction to R from low energy $e^+e^- \to q\bar{q}$ data.
- m_t enters basically through the corrections $\Delta\rho$ and $\Delta_{b\bar{b}\ vertex}$ in which the dependence is quadratic. From direct searches [10] we know that $m_t > 86$ GeV at the 95% C.L.
- m_H enters very weakly in the predictions because the dependence is just logarithmic. From direct search in our experiment the lower bound is $m_H > 42$ GeV [11] whereas unitarity arguments from the theoretical side suggest $m_H < 1$ TeV [12].
- N_ν introduces a very strong dependence in some observables which therefore can be used to determine it. In the Standard Model, N_ν is bound to be integer and then usually the predictions are quoted for $N_\nu = 2, 3, 4$.

There are two different ways of facing the comparison of the measured quantities with the Standard Model predictions:

- 1.- Asume the Standard Model predictions to study the range of allowed values for the unknown parameters (m_t,m_H).
- 2.- Analyze observables which do not depend on the unknown parameters (or depend very weakly). By comparing these observables with the Standard Model predictions, the aim is checking the internal structure of the theory rather than determining the unknown parameters.

In the first way, a part from M_Z we measure three additional quantities which, given the fact that depend on the unknown quantities can be used

$$\begin{aligned} \Gamma_Z &\simeq \Gamma_Z(\alpha_s, m_t, m_H, N_\nu) \\ \Gamma_l &\simeq \Gamma_l(m_t, m_H) \\ \Gamma_h &\simeq \Gamma_h(\alpha_s, m_t, m_H) \end{aligned}$$

the contour plots of our measured values contrasted with the Standard Model predictions for different top masses can be seen in figs. 8 and 9. From these plots the top mass range favored by our measurements can be clearly seen.

In the second way, it is worth noting that in the ratios of partial widths the dependence on m_t and m_H cancels in good approximation. Therefore we can also express our measurements in terms of the following quantities:

$$\begin{aligned} R &\equiv \frac{\Gamma_h}{\Gamma_l} \simeq R(\alpha_s) \\ \sigma_0^h &\equiv \frac{12\pi}{M_Z^2}\frac{\Gamma_l\Gamma_h}{\Gamma_Z^2} \simeq \sigma_0^h(\alpha_s, N_\nu) \\ R_\nu &\equiv \frac{\Gamma_{inv}}{\Gamma_l} \simeq R_\nu(N_\nu) \end{aligned}$$

Table 4 and figures 10 and 11 show the comparison between our measurements and the Standard Model predictions. No indication of disagreement can be seen in any measurement.

Observable	Measurement	S.M. prediction
R	21.07 ± 0.19	20.79 ± 0.08
σ_0^h	41.76 ± 0.39 nb	41.43 ± 0.07 nb
R_ν	5.78 ± 0.16	5.974 ± 0.012

Table 4: Comparison of the measured values of the ratios with the S.M. predictions.

5 Interpretation assuming the Standard Model

Assuming the minimal Standard Model structure, one can combine the above measurements to extract information about basic parameters of the theory.

5.1 Determination of the number of neutrino species

As seen in the plots shown in the previous section, N_ν, the number of neutrino species can be extracted from σ_0^h and R in a top mass independent way. By solving the following system of equations

$$\begin{cases} \sigma_0^h = \frac{12\pi}{M_Z^2}\frac{\Gamma_l\Gamma_h}{\Gamma_Z^2} \\ \\ \Gamma_Z = \Gamma_h + 3\Gamma_l + N_\nu\Gamma_\nu \end{cases} \tag{22}$$

one trivially obtains

$$N_\nu = \frac{\Gamma_l}{\Gamma_\nu}\cdot\left[\left(\frac{12\pi}{M_Z^2}\frac{R}{\sigma_0^h}\right)^{\frac{1}{2}} - R - 3\right] \tag{23}$$

that is, the number of neutrinoes is obtained in terms of ratios and thus in a way unsensitive to the top mass value. We use the very precise Standard Model prediction:

$$\frac{\Gamma_l}{\Gamma_\nu}(S.M.) = 0.5022 \pm 0.0010$$

together with our measured values of M_Z, σ_0^h and R to obtain

$$N_\nu = 2.90 \pm 0.08$$

5.2 Determination of the universal effective weak mixing angle

The universal effective weak mixing angle $\sin^2\theta_W(M_Z^2)$ can be considered as a parameter which contains in a very precise way the genuine new information coming from the asymmetry measurements. Anyway, for the reason of comparison of the relative accuracies of different measurements, it is interesting trying to express also the lineshape measurements in terms of the same quantity. This is done by using the relation

$$\Gamma_l = (1+\kappa)\ \frac{M_Z\alpha(m_z^2)}{48}\ \frac{1+(1-4\sin^2\theta_W(M_Z^2))^2}{\sin^2\theta_W(M_Z^2)\cos^2\theta_W(M_Z^2)} \tag{24}$$

where the factor $\kappa = (0.2\pm0.3)\%$ collects residual corrections and the remaining dependence on m_t and m_H [13]. From our measured value of Γ_l we obtain

$$\text{From } \Gamma_l \implies \sin^2\theta_W(M_Z^2) = 0.2325 \pm 0.0025$$

From the forward-backward lepton charge asymmetry we have seen that we extract directly

$$(\sin^2\theta_W)_l = 0.2274 + 0.0040 - 0.0036$$

This effective quantity can be related to the universal effective weak mixing angle by just doing the following shift:

$$(\sin^2\theta_W)_l = \sin^2\theta_W(M_Z^2) + 0.0007$$

which is due to the effect of vertex corrections mainly (and therefore does not depend on m_t or m_H). Thus, from or measured values of A_{FB} we have

$$\text{From } A_{FB} \implies \sin^2\theta_W(M_Z^2) = 0.2267 + 0.0040 - 0.0036$$

If we combine both measurements we end up with

$$\sin^2\theta_W(M_Z^2) = 0.2309 \pm 0.0020$$

6 Combination with other precision measurements

We can combine our precision measurements with other existing ones in order to check the consistency with these measurements, and at the same time obtain better constraints on the top mass.

The most relevant additional accurate information about the Electroweak sector, comes from direct measurement of M_W in $p\bar{p}$ colliders [14] and from the measurement of $\sin^2\theta_W$ in neutrino-nucleon scattering experiments [15]. These measurements can be compiled in the following value of the mass ratio

$$\sin^2\theta_W = 1 - \frac{M_W^2}{M_Z^2} = 0.2292 \pm 0.0042 \tag{25}$$

In the minimal Standard Model for three neutrino species, any observable can be computed as a function

$$f = f(M_Z, m_t, m_H, \alpha_s) \tag{26}$$

Specifically, the universal effective mixing angle can be expressed as

$$\sin^2\theta_W(M_Z^2) = \sin^2\theta_W(M_Z, m_t, m_H, \alpha_s) \tag{27}$$

and therefore by inverting this equation we can write

$$M_Z = M_Z(\sin^2\theta_W(M_Z^2), m_t, m_H, \alpha_s) \tag{28}$$

Since M_Z is in fact one of the measurements from which we would like to analyze the information contained, we can substitute it in this set of variables for the effective mixing angle: $M_Z \to \sin^2\theta_W(M_Z^2)$ and therefore we have reparametrized any prediction in terms of

$$f = f(\sin^2\theta_W(M_Z^2), m_t, m_H, \alpha_s) \tag{29}$$

so that we can analyze which information about m_t and about the bookkeeping parameter $\sin^2\theta_W(M_Z^2)$ does each measurement contain. For that we proceed in the following way: fixing a value of m_H, for any given m_t we solve the equations

$$f + \Delta f = f(\{\sin^2\theta_W(M_Z^2)\}_+, m_t, m_H, \alpha_s)$$
$$f - \Delta f = f(\{\sin^2\theta_W(M_Z^2)\}_-, m_t, m_H, \alpha_s)$$

The uncertainty in α_s is treated by adding quadratically the variation in $\sin^2\theta_W(M_Z^2)$ due to a change in α_s with the one coming from the uncertainty of the measurement itself.

The plot obtained by applying this procedure to our measurements and the ones of the mass ratio, is shown for different values of m_H in figure 12. In this plot, the dashed bands correspond to the 1σ region limited by each measurement in the plane m_t versus $\sin^2\theta_W(M_Z^2)$ for a given value of m_H.

We can perform a χ^2 fit using all the data. For that, since the dependence on m_H with the present level of accuracy is very weak, we fix m_H and use as fitting parameters m_t, $\sin^2\theta_W(M_Z^2)$ and α_s. The χ^2 is then defined as

$$\chi^2 = \sum_1^{N_m} \left(\frac{f_{meas.} - f(\sin^2\theta_W(M_Z^2), m_t, m_H, \alpha_s)}{\Delta f_{meas.}}\right)^2 \tag{30}$$

where N_m denotes the total number of measurements used. In our case, these measurements are:

- from the lineshape: M_Z, Γ_Z and Γ_l
- from the asymmetry: $\sin^2\theta_W(M_Z^2)$
- from other precision experiments: $\sin^2\theta_W = 1 - \frac{M_W^2}{M_Z^2}$
- from low energy $e^+e^- \to q\bar{q}$ data: α_s

in addition a penalty function has been included in the fit to account for the CDF limit $m_t > 86$ GeV. The results of the fits are summarized in table 5. The χ^2 per degree of freedom is of 3.7/5 so that no disagreement between the different measurements with the Standard Model predictions can be pointed out.

	$m_H = 200$ GeV	$m_H = 50$ GeV	$m_H = 1$ TeV
m_t(GeV)	$142 + 30 - 35$	-15	$+22$
$\sin^2\theta_W(M_Z^2)$	0.2322 ± 0.0010	-0.0003	$+0.0002$

Table 5: Results of the fits to m_t

7 Conclusions

By studying the Z decay events collected in the ALEPH detector in the runs of 1989 and 1990 we have measured the following Z properties:

$$M_Z = (91.182 \pm 0.009_{exp} \pm 0.02_{LEP}) \text{ GeV}$$
$$\Gamma_Z = (2.488 \pm 0.017) \text{ GeV}$$

$$
\begin{aligned}
\Gamma_h &= (1756 \pm 15)\ \text{MeV} \\
\Gamma_{inv} &= (481 \pm 14)\ \text{MeV} \\
\Gamma_e &= (84.2 \pm 0.9)\ \text{MeV} \\
\Gamma_\mu &= (80.9 \pm 1.4)\ \text{MeV} \\
\Gamma_\tau &= (82.9 \pm 1.6)\ \text{MeV} \\
\Gamma_l &= (83.3 \pm 0.7)\ \text{MeV}
\end{aligned}
$$

$$
\begin{aligned}
(g_v^l)^2 &= 0.00203 \pm 0.00065 \\
(g_a^l)^2 &= 0.2484 \pm 0.0022
\end{aligned}
$$

All the measurements show good agreement with the Standard Model predictions. Furthermore, assuming the minimal Standard Model we have determined

$$
\begin{aligned}
N_\nu &= 2.90 \pm 0.08 \\
\sin^2\theta_W(M_Z^2) &= 0.2309 \pm 0.0020
\end{aligned}
$$

Our measurements compare well with precision measurements performed in other machines. The combination of the measurements enables us to determine the top mass to be

$$m_t = 142 + 30 - 35 \quad (+22 - 15)_{m_H}\ \text{GeV}$$

Acknowledgments

I thank all the members of the ALEPH collaboration for their help and encouragement in performing a conscious work and also for providing all the necessary information for the completion of this manuscript.

References

[1] D. Decamp et al., ALEPH: Nuclear Instruments and Methods A294 (1990) 121

[2] D. Decamp et al., ALEPH: Z. Phys. C - Particles and Fields 48, (1990) 365. The description of the final analysis applied is still in preparation.

[3] M. Martinez and R. Miquel : Fitting the $e^+e^- \to e^+e^-$ lineshape, CERN-PPE in preparation.

[4] F.A. Berends, W. Beenakker and S. van der Mark: Nucl. Phys. B349 (1991) 323

[5] F.A. Berends, G. Burgers and W.L. van Neerven: Nucl. Phys. B297 (1988) 429; ibid B304 (1988) 921

[6] M. Martinez et al.: Model Independent Fitting to the Z Line Shape, CERN-PPE/90-109 , to appear in Z. Phys. C - Particles and Fields ; see also references therein

[7] D.C. Kennedy, B.W. Lynn: Nucl. Phys. B322 (1989) 1 ; M. Consoli, W. Hollik, F. Jegerlehner: in Proceedings of the Workshop of Z Physics at LEP, CERN Reports 89-08, 1989, vol. I, 7 ; W.J. Marciano and A. Sirlin: Phys. Rev. Lett. 46 (1981) 163

[8] S. Jadach and Z. Wąs: MPI-PAE/PTH 33/89, 34/89 (1989)

[9] M. Böhm, W. Hollik: in Proceedings of the Workshop of Z Physics at LEP, CERN Reports 89-08, 1989, vol. I, 203

[10] F. Abe at al., CDF: Phys. Rev. Lett. 64(2):147, 1990; K. Sliwa in: Proceedings of the XXVth Rencontres de Moriond, March 1990.

[11] D. Decamp et al., ALEPH: Phys. Lett. B246 (1990) 306

[12] R. Kleiss in: Electroweak interactions, Lecture Series for Postgraduate Students, 1990-1991 Academic Training Programme CERN.

[13] κ has been computed using the programs EXPOSTAR (from D.C. Kennedy et al.:Nucl. Phys. B321 (1989) 83) and GAMMAZ (from G. Burgers and W. Hollik based upon: W. Beenakker and W.Hollik: Z. Phys. C - Particles and Fields 40 (1988) 141)

[14] J. Alitti et al., UA2: Phys. Lett. B241 (1990) 150; F. Abe et al., CDF: ANL-HEP-PR-90-72 (1990)

[15] A. Blondel et al., CDHS: Z. Phys. C - Particles and Fields 45 (1990) 361; J.V. Allaby et al. CHARM: Z. Phys. C - Particles and Fields 36 (1987) 611

List of Tables

List of Figures

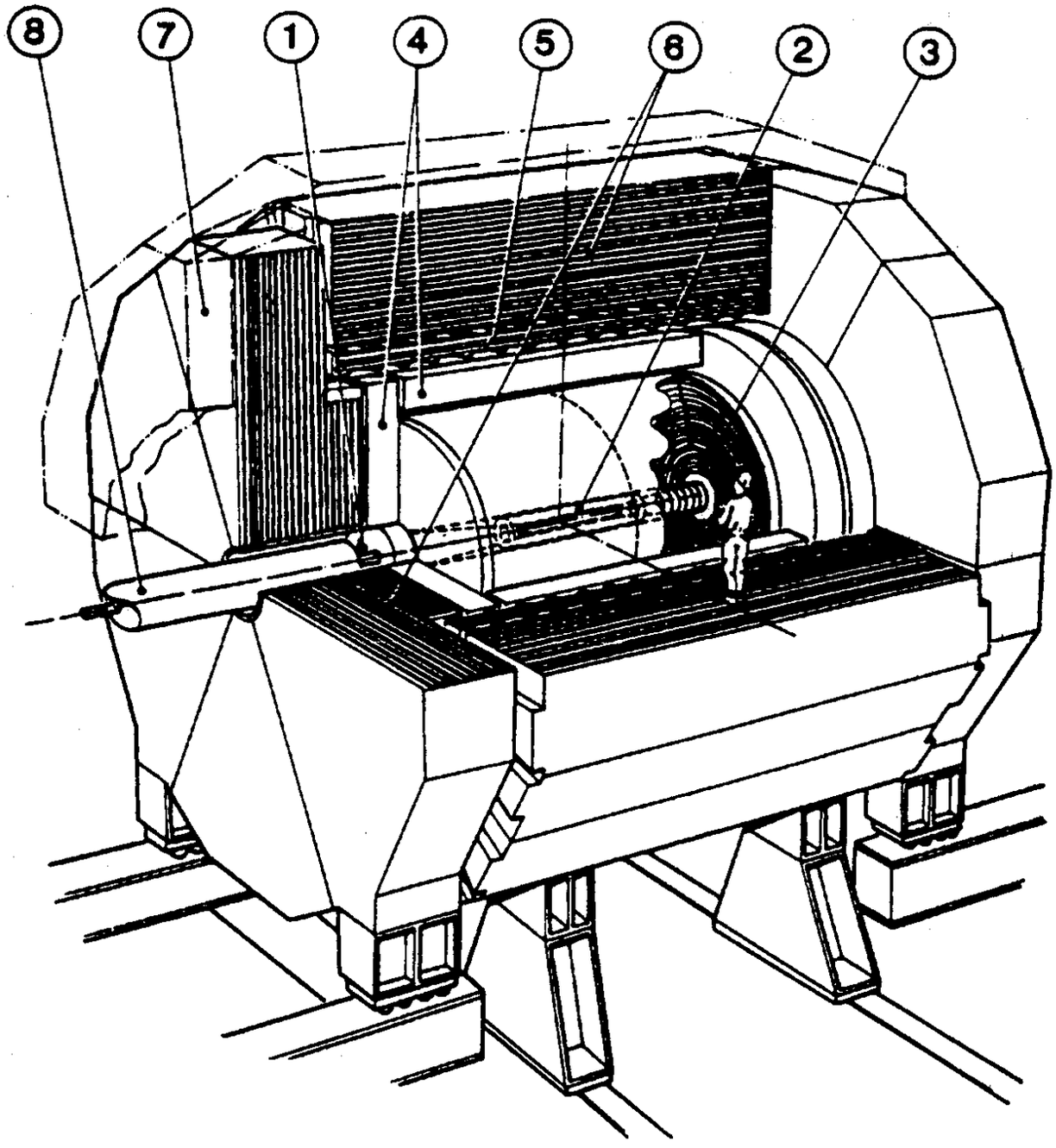

Figure 1: Schematic view of the ALEPH detector. (1) Luminosity Monitor. (2) Inner Tracking Chamber. (3) Time Proportional Chamber. (4) Electromagnetic Calorimeter. (5) Superconducting Coil. (6) Hadronic Calorimeter. (7) Muon Chambers. (8) Beam Pipe.

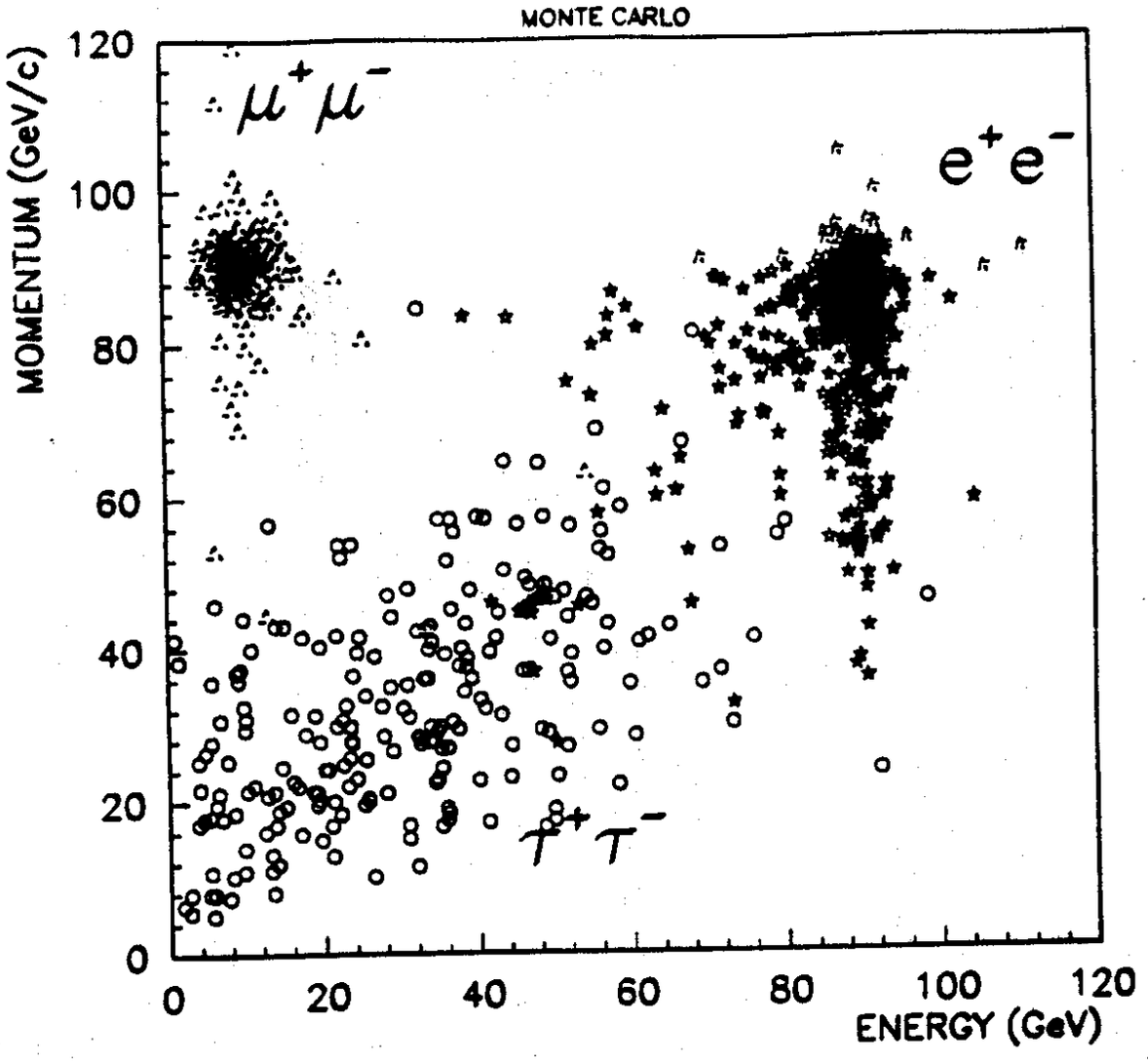

Figure 2: Visible momentum and energy spectrum of leptonic events from Monte Carlo data. The abscissa correspond to the total energy deposited in the calorimeters by the event and the ordinate correspond to the sum of the momenta of the two higher momentum tracks. The Monte Carlo data correspond to a $\mathcal{L} = 180\ nb^{-1}$ of e^+e^-, $\mu^+\mu^-$ and $\tau^+\tau^-$ events at $\sqrt{s} = 91.2$ GeV.

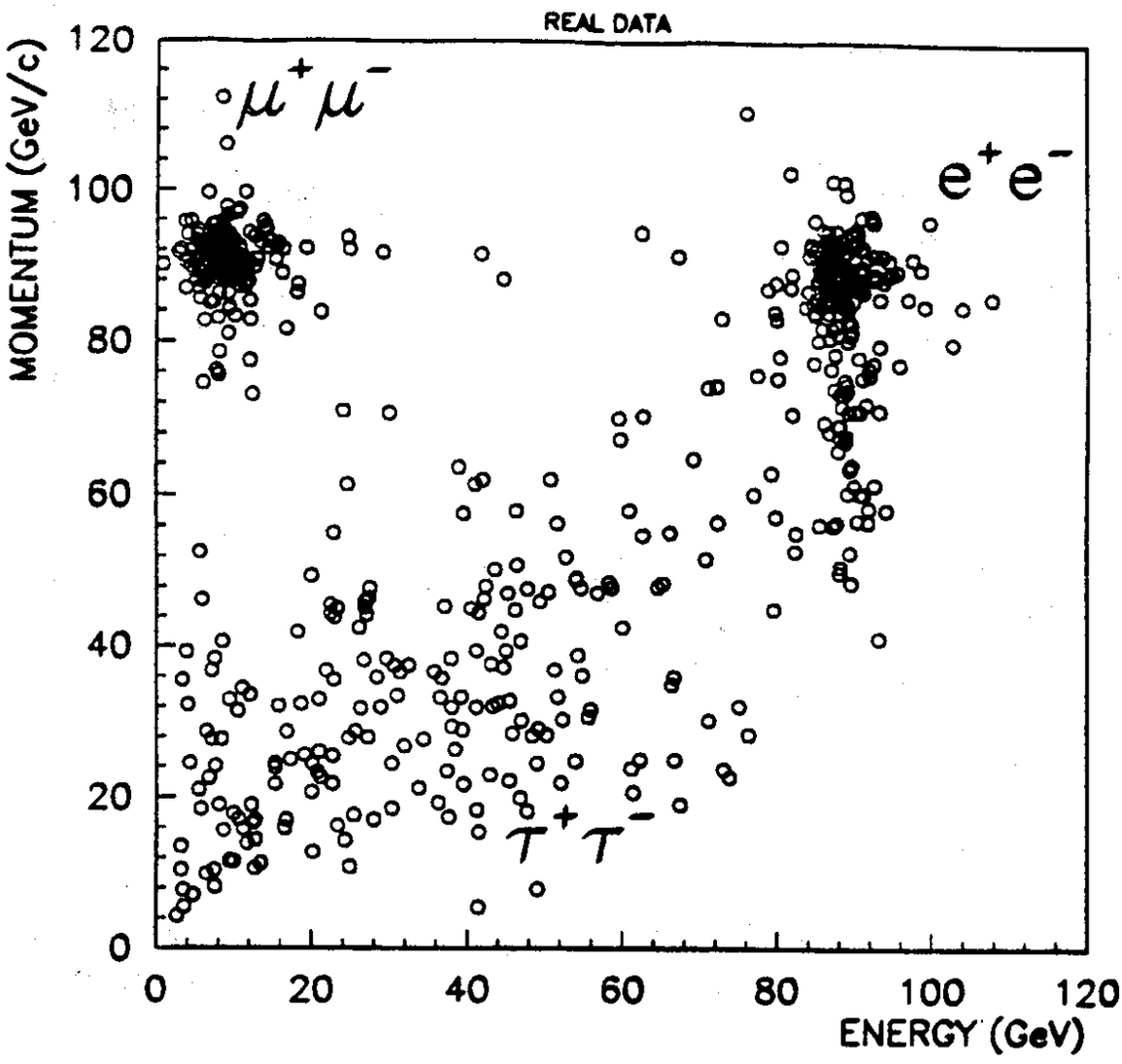

Figure 3: Visible momentum and energy spectrum of leptonic events from real data. The abscissa correspond to the total energy deposited in the calorimeters by the event and the ordinate correspond to the sum of the momenta of the two higher momentum tracks. The data correspond to a luminosity of 180 nb^{-1} of the 1990 data at $\sqrt{s} = 91.22$ GeV.

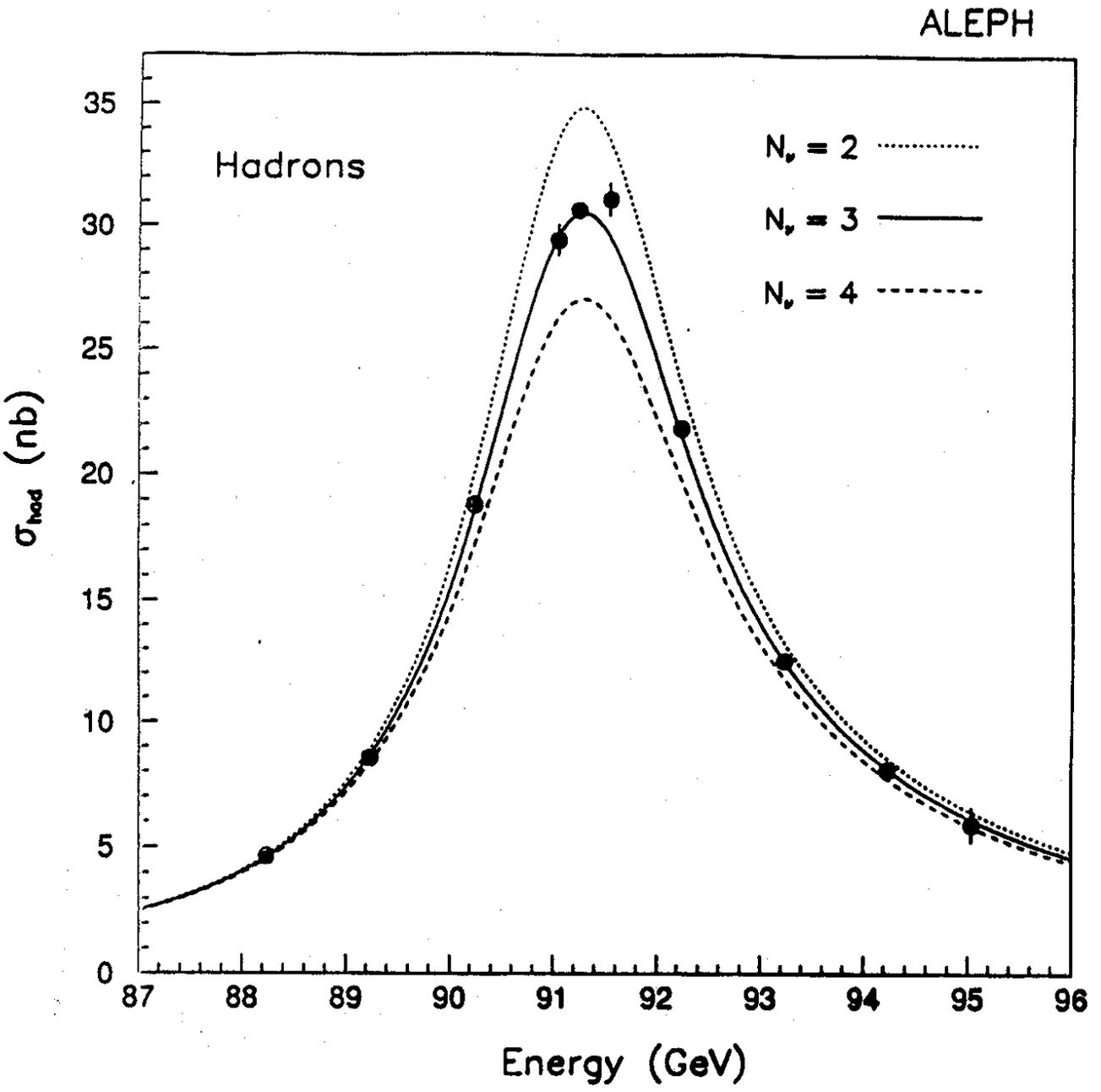

Figure 4: Hadronic lineshape. The solid line corresponds to the best fit. The cross sections corresponding to energy points close together have been combined.

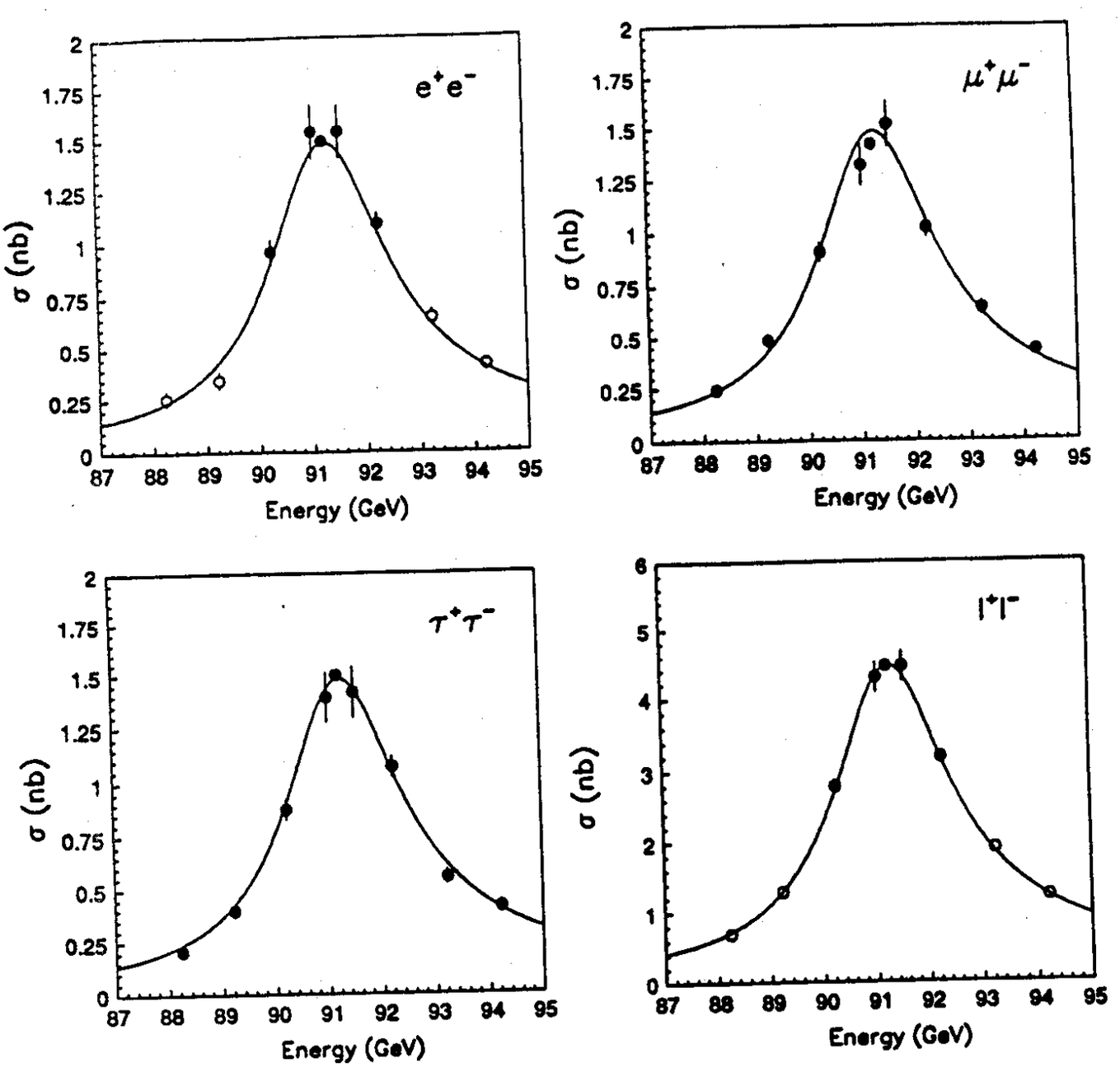

Figure 5: Leptonic lineshapes. The solid line corresponds to the best fit. The cross sections corresponding to energy points close together have been combined. The points corresponding to white dots are not used at fitting time.

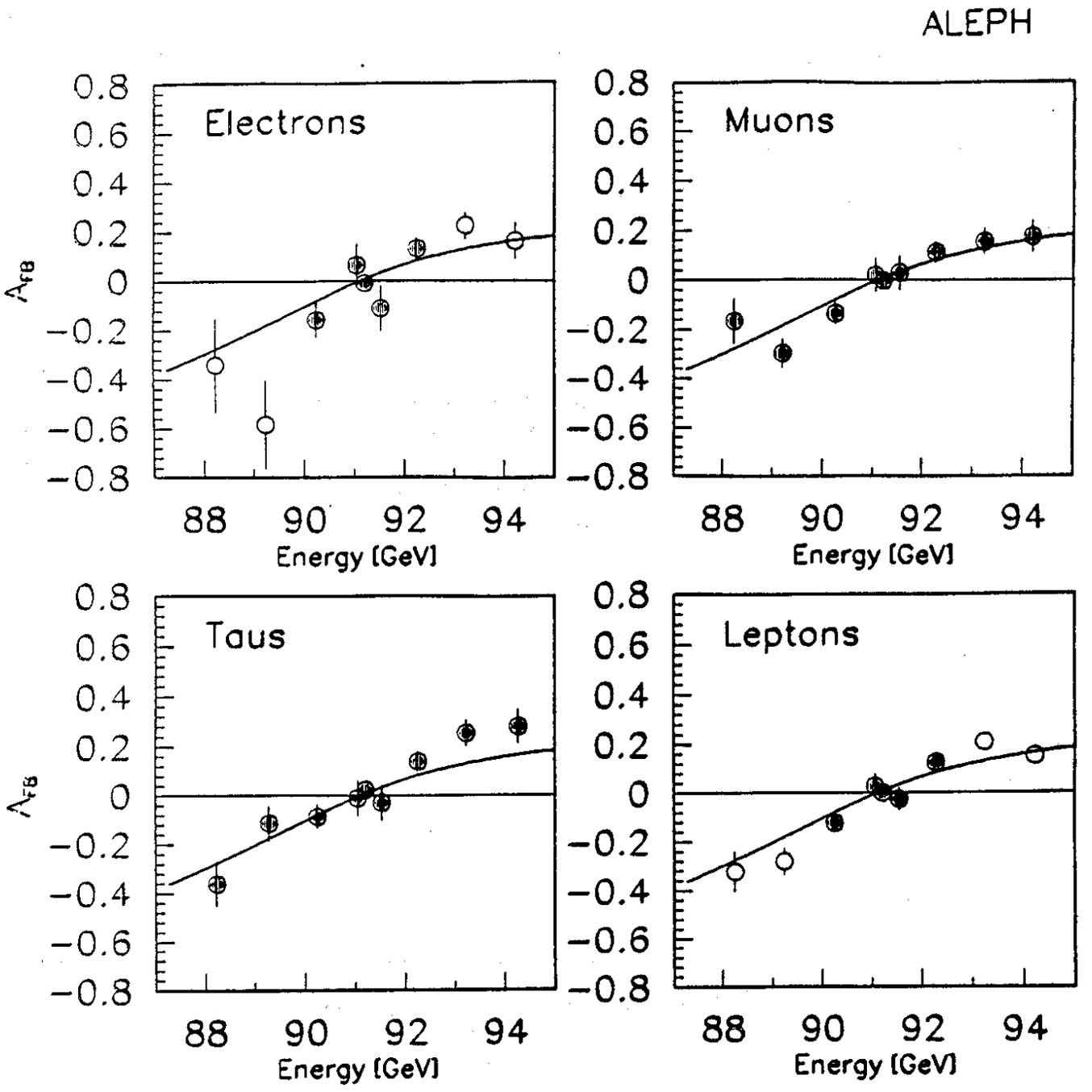

Figure 6: Leptonic forward-backward charge asymmetry. The solid line corresponds to the best fit. The points corresponding to white dots are not used at fitting time.

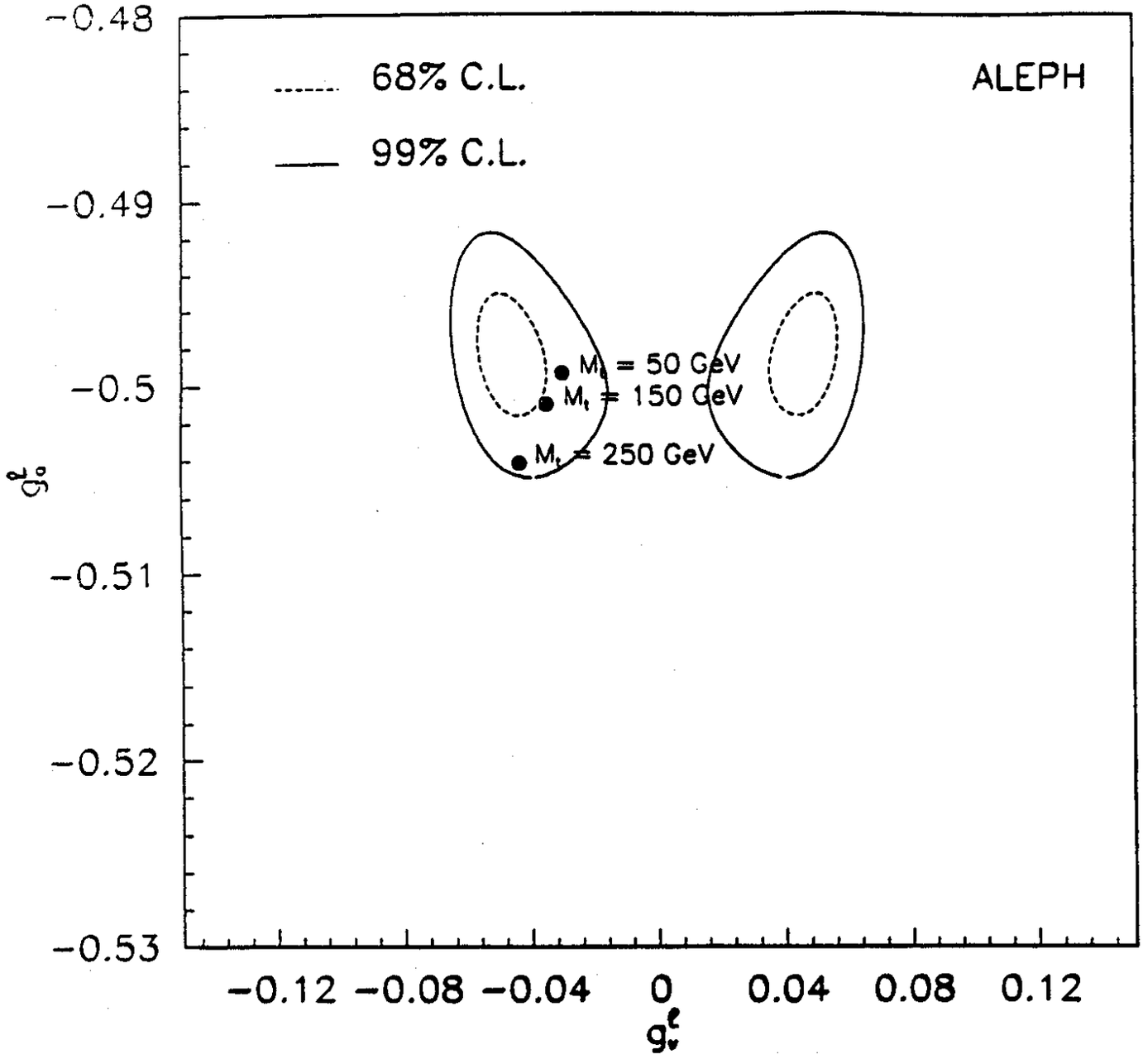

Figure 7: g_a versus g_v plot. The dots indicate the Standard Model predictions for different top masses.

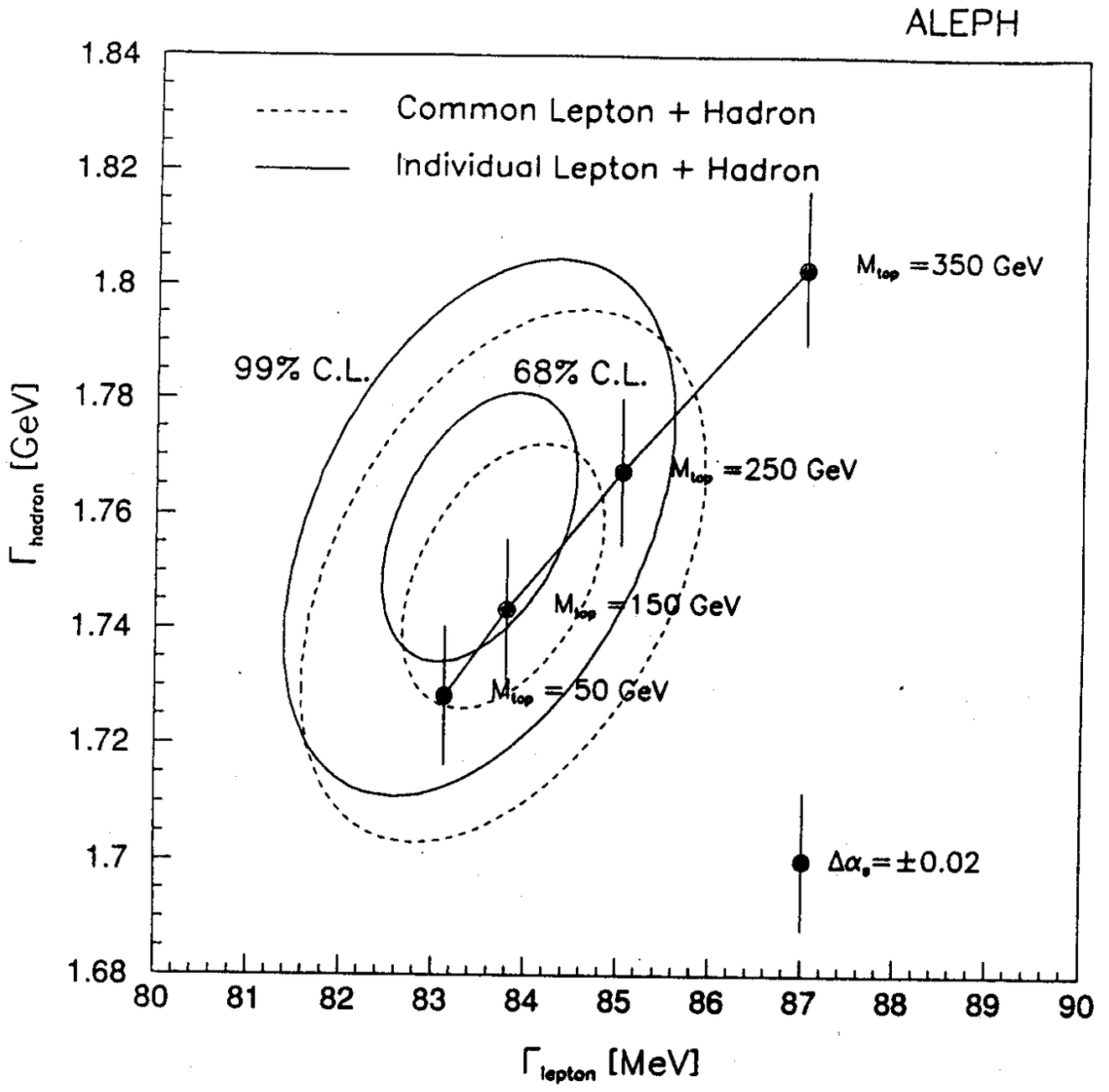

Figure 8: Γ_h versus Γ_l plot. The solid line indicates the contours obtained from the fit of the individual lepton lineshapes whereas the dashed one corresponds to the contours from the common lepton lineshape fit. The comparison with the Standard Model predictions shows the top mass range prefered by our Γ_h and Γ_l measurements.

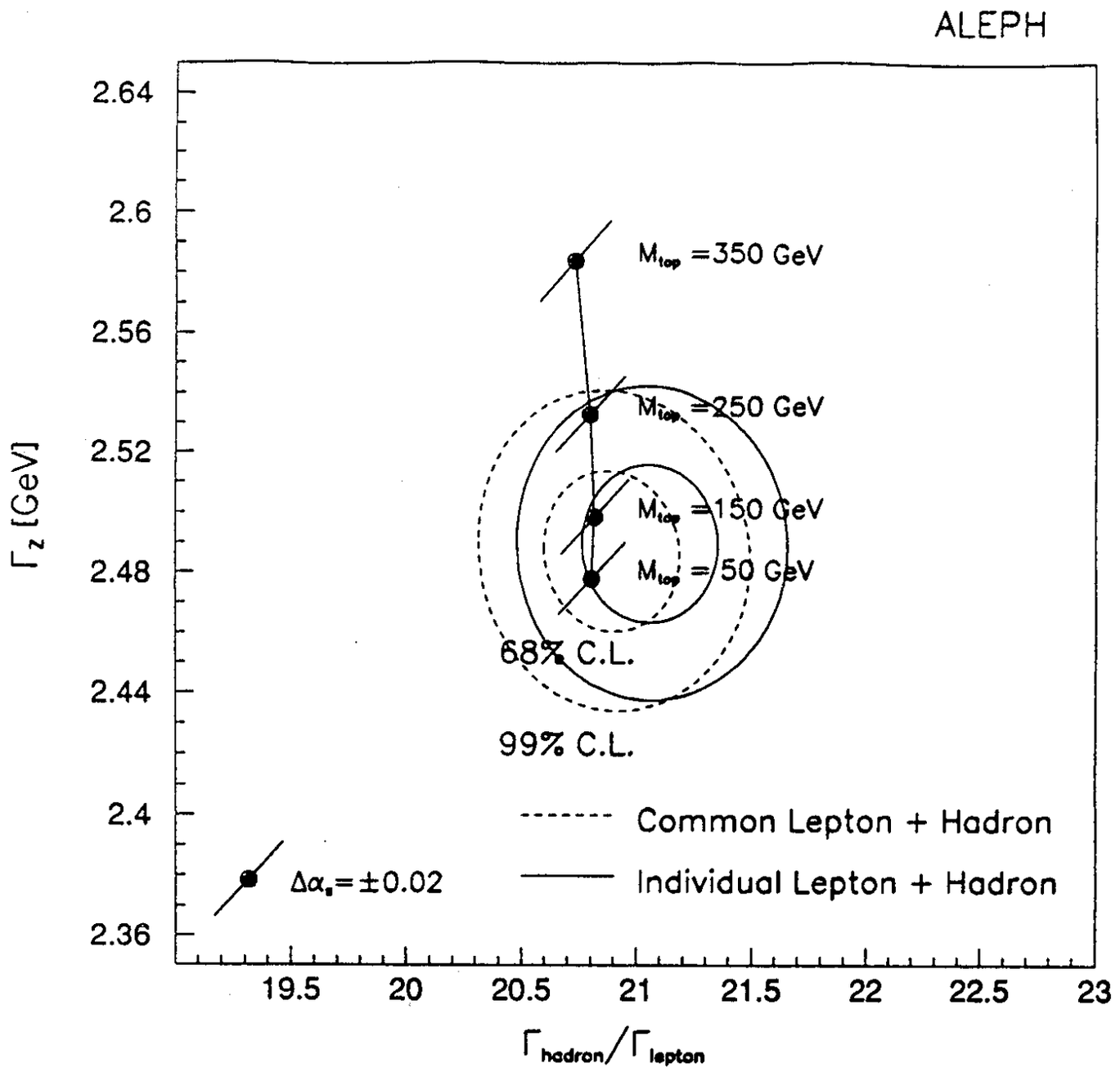

Figure 9: Γ_Z versus R plot. The solid line indicates the contours obtained from the fit of the individual lepton lineshapes whereas the dashed one corresponds to the contours from the common lepton lineshape fit. The comparison with the Standard Model predictions shows the top mass range prefered by the Γ_Z measurement.

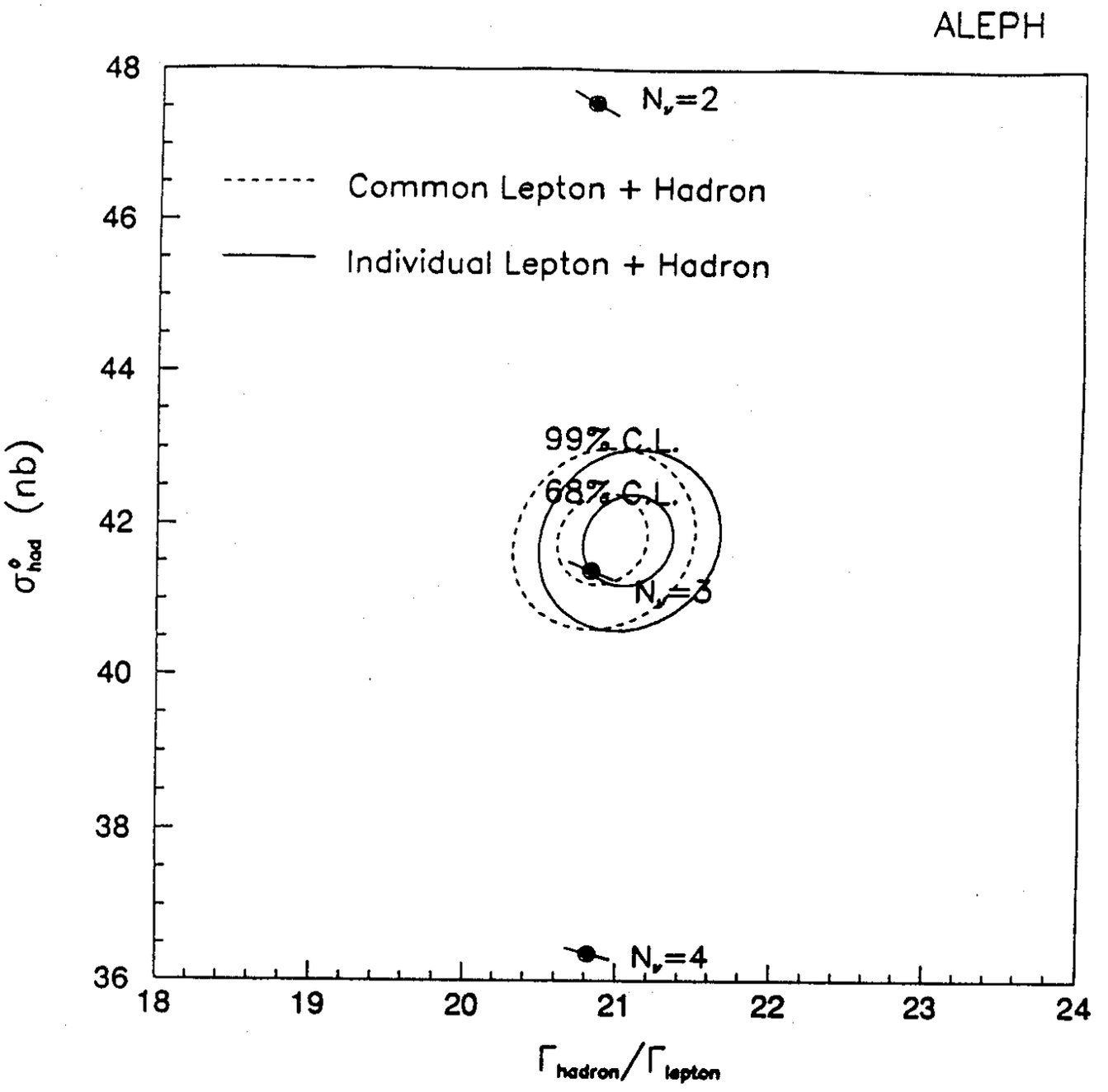

Figure 10: σ_0^h versus R plot. The solid line indicates the contours obtained from the fit of the individual lepton lineshapes whereas the dashed one corresponds to the contours from the common lepton lineshape fit.

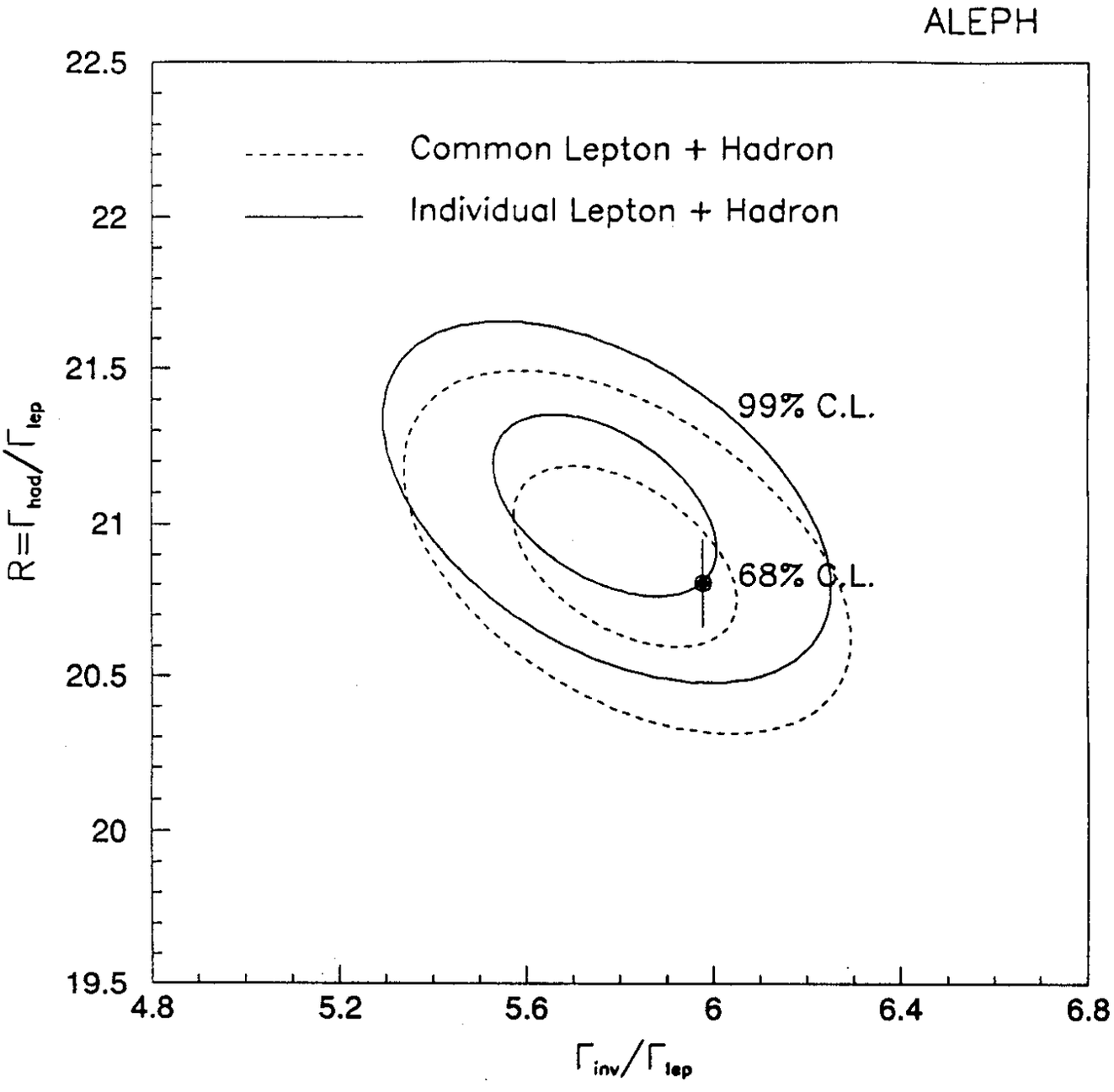

Figure 11: R versus $\frac{\Gamma_{inv}}{\Gamma_l}$ plot. The solid line indicates the contours obtained from the fit of the individual lepton lineshapes whereas the dashed one corresponds to the contours from the common lepton lineshape fit.

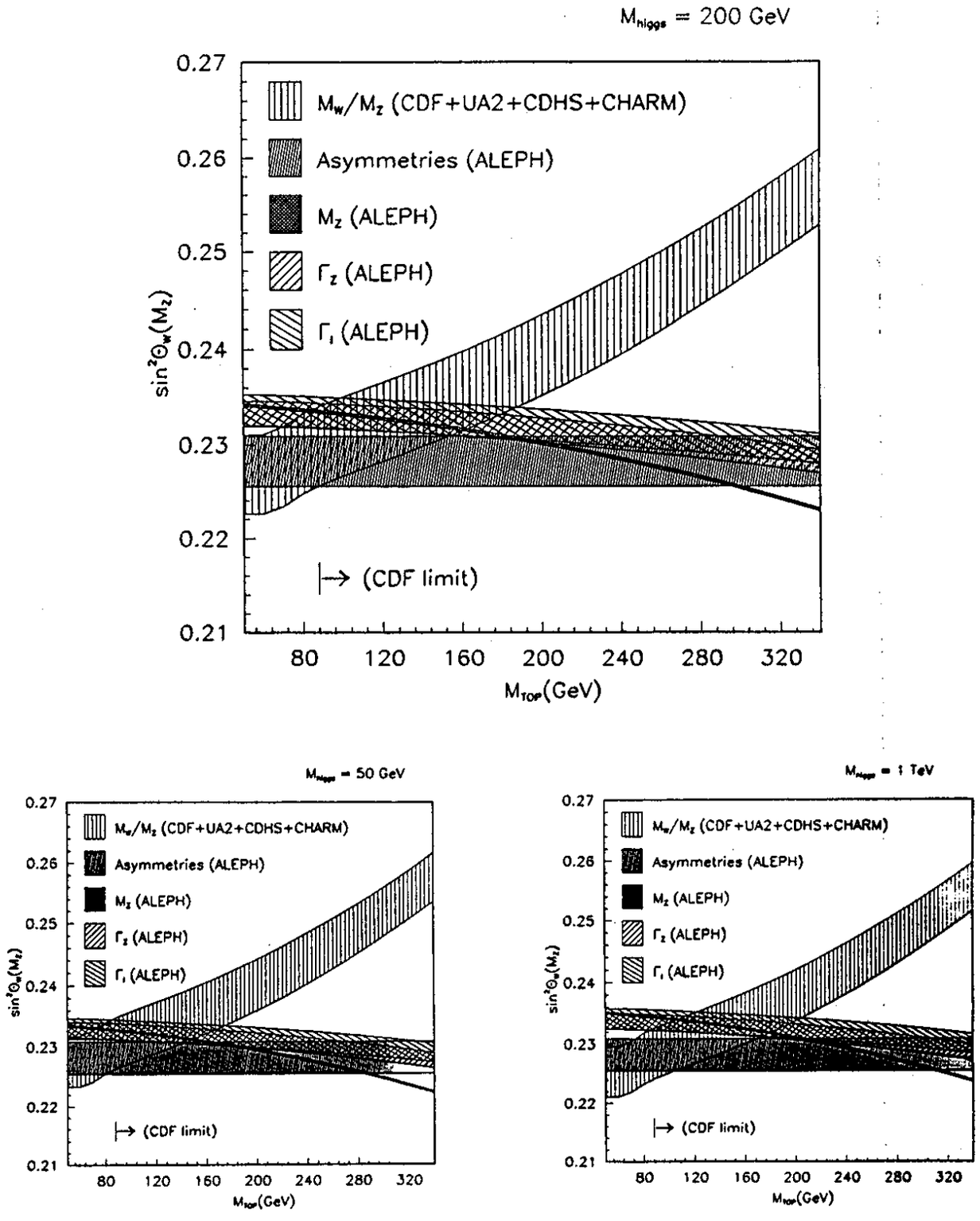

Figure 12: $\sin^2\theta_W(M_Z^2)$ versus m_t plot for three different values of m_H. The dashed region delimited by each measurement indicates the 1 σ allowed values of $\sin^2\theta_W(M_Z^2)$ as a function of m_t.